Winter 2017

CHIRAL BIOMOLECULE-INDUCED CHIROPTICAL ACTIVITY IN QUANTUM DOTS

Benjamin Haynie
University of New Hampshire, Durham

CHIRAL BIOMOLECULE-INDUCED CHIROPTICAL ACTIVITY IN QUANTUM DOTS

BY

BENJAMIN HAYNIE

Bachelor of Science in Chemistry, Louisiana Tech University, 2014

THESIS

Submitted to the University of New Hampshire

in Partial Fulfillment of

the Requirements for the Degree of

Master of Science

in

Biochemistry

December, 2017

This thesis has been examined and approved in partial fulfillment of the requirements for the degree of Master of Science in Biochemistry by:

Thesis Director, Dr. Krisztina Varga, Assistant Professor of Biochemistry

Dr. Rick Cote, Professor and Chair of Molecular, Cellular, and Biomedical Sciences

Dr. Christine Caputo, Assistant Professor of Chemistry

On August 22nd, 2017

Original approval signatures are on file with the University of New Hampshire Graduate School.

DEDICATION

I would like to dedicate this thesis to my parents, Sally and Howard Haynie; my siblings Andrew, Kelley, and Carrie; my close friends Chris Nordyke, Colleen Ricci, Cassidy Grice, and Erin McCowan Simpson; my girlfriend Jennifer Hazelton; and my former teacher Dr. Dena Leggett, along with the several other influential people in my life, for reasons both known and unknown to each of them. They have each molded and guided me to what and where I am today. It's safe to say that without their impact, be it small or large, my life would be immeasurably different. I offer my sincere gratitude to each of you.

ACKNOWLEDGEMENTS

I would like to thank first my advisor, Dr. Krisztina Varga, for her leadership and aid with this project, and especially for her patience and flexibility in accommodating the abrupt changes this project has faced. I have learned innumerable lessons of value from her guidance, for which I am eternally grateful. Many thanks to my thesis committee members, Dr. Rick Cote and Dr. Christine Caputo, for their participation in this process. They have been exceedingly accommodating with their schedules and availability through many changes.

I would also like to thank Dr. Milan Balaz for pioneering this project, as well as for his continued support and advice throughout my time here. There's no doubt his input and collaboration were vital to the project's continuing success. Additionally, I would like to acknowledge the work done by former Balaz group members, Dr. Jung Kyu Choi and Dr. Urice Tohgha, who started me on my work with this project in my first months as a graduate student. Further assistance came from Shambhavi Tannir, who continued to collaborate on the project after a hectic period of transition. I would like to acknowledge Mr. K. Wade Elliot (NMR) and Mr. Levente Pap for their help on the project.

This research was supported in part by the National Science Foundation grants CBET-1403947 and DGE-0948027.

Finally, I would like to thank the following collaborators from the University of Wyoming: Dr. Jan Kubelka (computational modeling and calculations), Dr. Brian Leonard (TEM, XRD), and Dr. Navamoney Arulsamy (XRD), for the work listed, as well as for their personal support:

Table of Contents

DEDICATION iii

ACKNOWLEDGEMENTS iv

LIST OF FIGURES vi

LIST OF TABLES viii

ABSTRACT ix

PROJECT HYPOTHESIS AND AIMS x

CHAPTER 1: INTRODUCTION TO QUANTUM DOTS 1

CHAPTER 2: INDUCED CHIRALITY WITH THIOL-CONTAINING LIGANDS 12

CHAPTER 3: REACTIONS WITH THIOL-FREE LIGANDS 22

CONCLUSION 32

CHAPTER 4: METHODS AND MATERIALS 33

LIST OF REFERENCES 36

LIST OF FIGURES

Figure 1: Physical properties of CdSe QDs. 1

Figure 2: Energy diagram of semiconductor band gap 2

Figure 3: Exciton Bohr radius 3

Figure 4: Size-dependent band gap 4

Figure 5: Size-dependent absorption spectra of CdSe QDs.. 5

Figure 6: OA-CdSe synthesis method 6

Figure 7: QD fluorescent imaging. 8

Figure 8: QD fluorescence shift upon bacterial binding 8

Figure 9: First study of chiral QDs. 9

Figure 10: Collective point chirality of CdTe nanocrystal 10

Figure 11: First example of ligand-induced chirality.. 11

Figure 12: Cys binding to CdSe QD 13

Figure 13: Cys titration curve 14

Figure 14: Phase transfer ligand exchange reaction 15

Figure 15: L-Cys-CdSe precipitate 16

Figure 16: CD spectra of CdS functionalized by Cys derivates 18

Figure 17: CD spectra of CdSe functionalized by Cys derivates 19

Figure 18: CD spectra vary with concentration 20

Figure 19: *N*-acetyl-L-Cys binding modes. 21

Figure 20: MA titration curve 22

Figure 21: pH dependent reactions 23

Figure 22: pH optimization of L-MA reaction 23

Figure 23: MA binding to CdSe QDs 24

Figure 24: Time optimization of L-MA reaction. 25

Figure 25: Carboxylic reaction phase separation 26

Figure 26: CD spectra MA-CdSe 28

Figure 27: CD spectra of TA-CdSe 29

Figure 28: CD spectra of *N*-Ac-L-Asp-CdSe 30

Figure 29: Molecular structures of the chiral ligand systems examined. 31

LIST OF TABLES

Table 1: Summary of thiol-free ligands used. 29

ABSTRACT

CHIRAL BIOMOLECULE-INDUCED CHIROPTICAL ACTIVITY IN QUANTUM DOTS

by

Benjamin Haynie

University of New Hampshire, December 2017

Chiroptical activity in cadmium selenide (CdSe) and cadmium sulfide (CdS) quantum dots (QDs) has been induced by interactions with chiral capping ligands, either with thiol functional group containing biomolecules (*e.g.* cysteine) or 'thiol-free' biomolecules (*e.g.* malic acid). This induced chirality is theorized to be the result of electronic orbital hybridization between the QD and ligand, not from physical distortion of crystal structure. The polarity of the resulting circular dichroism (CD) spectra shows a 'mirror-image' between enantiomers of the same ligand. However, it is possible for two ligands of the same absolute configuration to induce mirror-image CD spectra, as is the case for L-homocysteine and *N*-acetyl-L-cysteine. This is theorized to be a result of the geometric arrangement of the ligands on the surface of the QD, as predicted by non-empirical *ab initio* simulations. Further, the functional groups present in the ligand play a role in the induction of chiroptical activity, possibly by affecting the binding geometry or orbital hybridization of the ligand. With this and continuing work, it may be possible to predict the ligand-induced chiroptical activity of these QDs, leading to the opportunity for rational design of chiral QDs and other nanomaterial systems.

PROJECT HYPOTHESIS AND AIMS

The working hypothesis for the project consists of two parts:

a. The structure of the ligand plays a key role in the induction of chiroptical activity by affecting the binding mode, binding geometry, and binding pattern of the ligand on the crystal surface.
b. Both the nature of the functional groups and their positions within the structure are important.

The aim for the project, in order to test the validity of this hypothesis, is to **determine the chiral ligand and quantum dot structural and electronic requirements for induction of chiroptical properties in quantum dots.** To that end, four questions guided the focus of our experimentation:

1. Can cysteine derivatives be used for induction of chirality in CdSe quantum dots?
2. Can L- and D-cysteine induce chirality in quantum dots made of other materials besides CdSe?
3. Can thiol-free ligands be used to induce chirality in quantum dots?
4. Does a difference in functional groups affect the ability of an otherwise structurally similar ligand to induce chirality in quantum dots?

CHAPTER 1: INTRODUCTION TO QUANTUM DOTS

For around 30 years, semiconductor nanocrystals known as quantum dots (QDs) have been studied for their unique optical properties. These nanocrystals are typically synthesized and studied as colloids in organic or aqueous solution (Figure 1)[1], although certain applications make use of purified and dried powders. A semiconductor in bulk behavior has two continuous electronic orbital bands, the valence band and the conduction band (Figure 2). The highest-energy valence band is the equivalent of the "highest occupied molecular orbital" (HOMO) in organic molecules, and the lowest energy conduction band corresponds to the "lowest unoccupied molecular orbital" (LUMO). The energy difference between these two states is called the bandgap (equivalent of the HOMO/LUMO gap), determined by the chemical composition of the crystal.

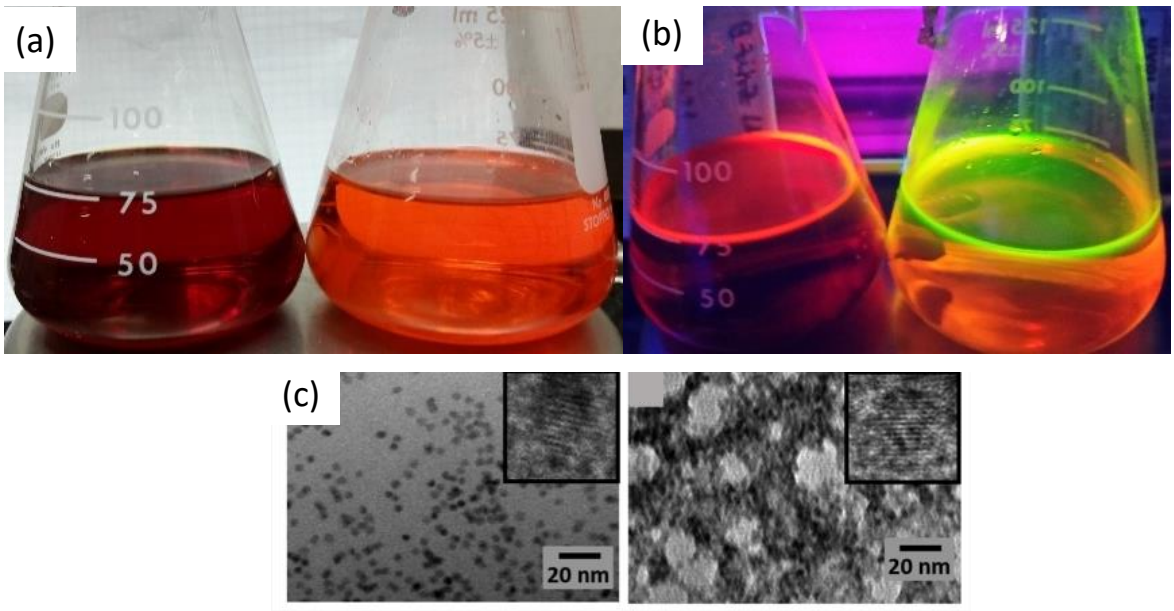

Figure 1: *Physical properties of CdSe QDs. (a) Colloidal oleic acid capped CdSe QDs in toluene. Solution color is determined by crystal size, where absorption wavelength increases with QD diameter. A diameter of 3.5 nm (left) appears red, while 2.5 nm QDs (right) appears orange. (b) QDs are fluorescent under UV illumination (375 nm). Emitted light wavelength is similarly proportional to QD diameter, with ~3.5 nm (left) fluorescing orange, and ~2.5 nm (right) green. (c) TEM imaging shows individual crystals of ~4.4 nm CdSe capped with N-Ac-L-Cys (left) and L-Homocys (right).*[1]

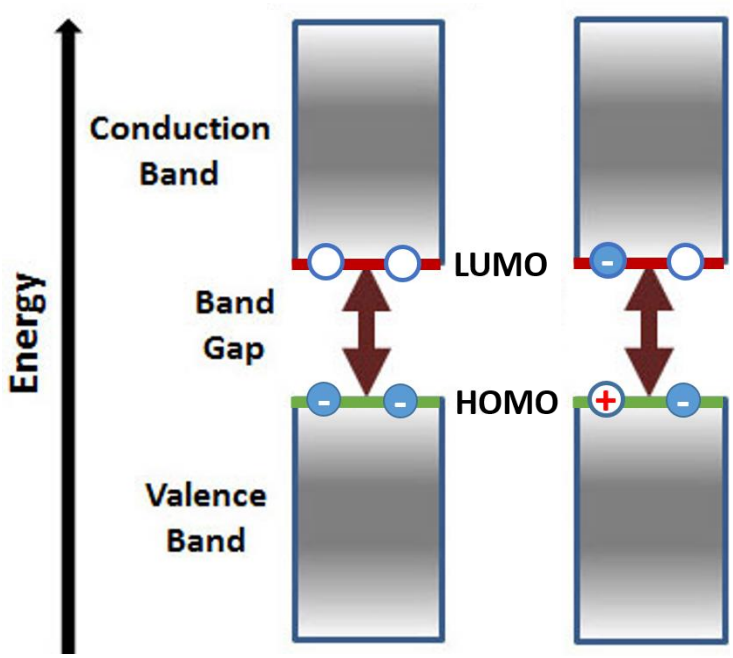

Figure 2: *Energy diagram of semiconductor bandgap during photoexcitation. In the ground state (left), the HOMO contains the valence electrons, while the LUMO is unoccupied. Upon excitation (right), an electron moves from the HOMO to the higher-energy LUMO, leaving behind a positively-charged hole.*

During excitation due to photoabsorption or electrical energizing, an electron from the valence band is excited to the conduction band, generating an electron hole in the valence band (Figure 2). This electron-hole pair, called an exciton, can be modeled similar to a hydrogen atom with the positively-charged hole replacing the nuclear proton (Figure 3). Using Bohr's equation, the expected radius of separation for this pair can be determined from the energy of the excitation (Equation 1). In the case of nanocrystals, however, when a semiconductor crystal has a radius less than the calculated Bohr radius of the bulk exciton, these bands become more quantumly discrete.[2]

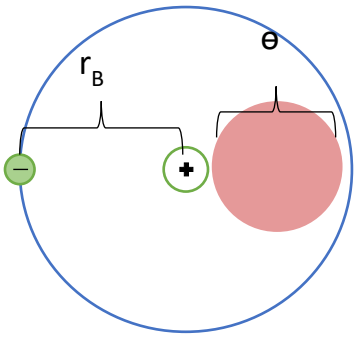

Figure 3: *An exciton is an electron/hole pair modeled similar to a hydrogen atom. The electron orbits at a radius, r_B, determined by the modified Bohr equation. When the crystal diameter (ϴ) is smaller than the Bohr radius of the exciton, the optically-active electrons become confined.*

$$r_B = \frac{\hbar^2 \mathcal{E}}{e^2}\left(\frac{1}{m_e} + \frac{1}{m_h}\right) \qquad (1)$$

Equation 1: *Bohr radius of exciton, where ħ is the Dirac constant, ε is the dielectric constant, m_e is the electron mass, and m_h is the exciton hole mass.*

This effect is due to the phenomenon of *quantum confinement*. If the excited electron is confined to a distance closer than the exciton Bohr radius (Figure 3), the electron is forced to take energies directly correlated to the amount of restriction from its desired radius (Equation 2).

$$E_{confinement} = \frac{\hbar^2 \pi^2}{2r^2}\left(\frac{1}{m_e} + \frac{1}{m_h}\right) \qquad (2)$$

Equation 2: *Energy of confinement, where r is the radius of confinement.*

Greater restriction requires more energy, therefore smaller QDs exhibit higher-energy excitations (Figure 4). But as the material grows, the confinement energy rapidly approaches zero, at which point the material exhibits bulk behavior.

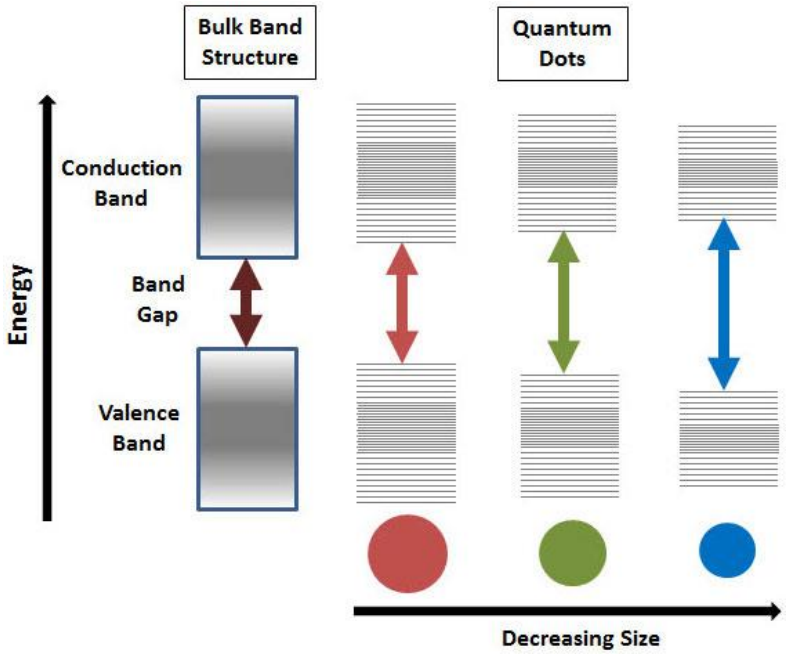

Figure 4: *As semiconductor crystals decrease in size, their confinement energy increases, widening the band gap. This causes particles of different sizes to absorb light of different energy and display different colors.*

Quantum confined materials display distinct excitonic peaks observed in the absorption spectra of these QDs, along with sharp emission peaks in the fluorescence spectra. The locations of these peaks shift according to the size of the particle, as the energy of excitation depends on the radius of the particle (Figure 5).[3]

The relationship between excitation energy and diameter has been expressed in empirical formulae for CdS, CdSe, and CdTe QDs by Peng (*i.e.*, the Peng equations) for diameter and extinction coefficient as a function of the first excitonic peak.[4] These equations are accurate for fatty acid or phosphonic acid QDs in a range of approximately D= 1-8 nm, well suited for a majority of colloidal QDs. These equations also provide a good estimate for the size of QDs with other ligand systems, although absorption peak location has been shown to be sensitive to ligand environment.

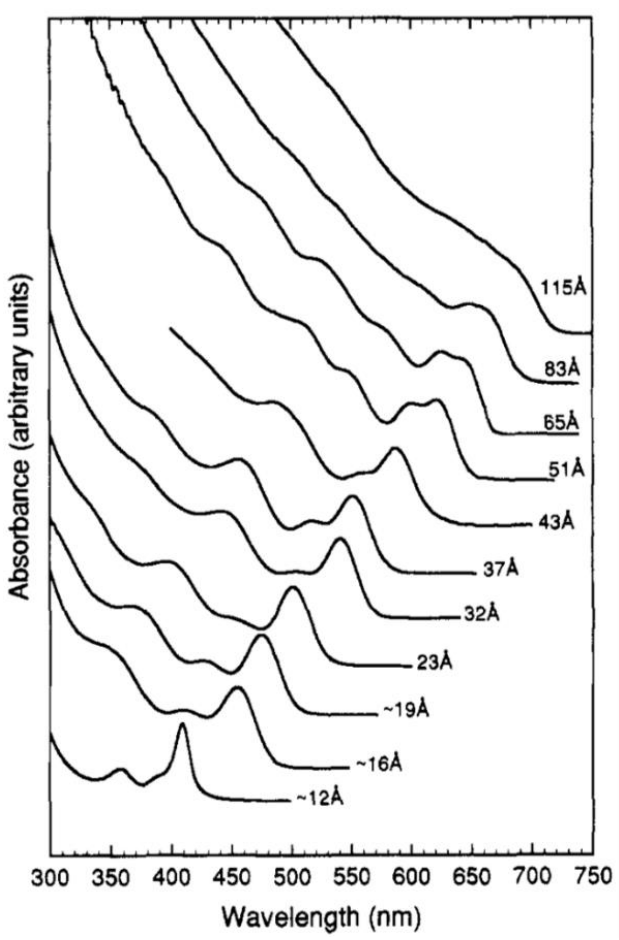

Figure 5: *Size-dependent absorption spectra of CdSe QDs.[3] Highly confined crystals exhibit sharp absorption peaks at high energy (short wavelength). As particle size increases, the exciton becomes less confined and at a lower energy, so the peak broadens and shifts to lower energies.*

Preparation of QDs can be done several different ways, but is commonly achieved through colloidal synthesis of organic solutions of the constituents.[5] This allows for safe, precise control over the size and quality of QDs while being cost-efficient. These processes have been scaled up to provide large-scale manufacture of commercially-used QDs. For my project, I used a modified version of a well- established synthetic procedure (Figure 6).

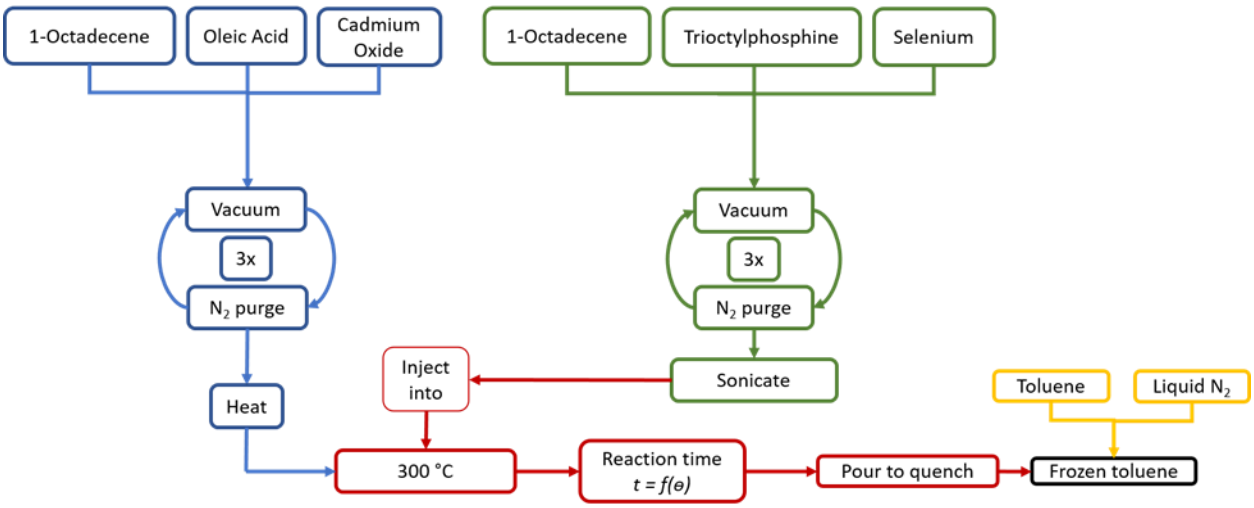

Figure 6: *Modified OA-CdSe synthesis method. Mixtures of oleic acid/CdO and TOP/Se are made separately. The CdO solution is heated under nitrogen to 300 °C. The TOPSe solution is then injected into the CdO flask, then quenched after growing to desired size.*

The unique optical properties of QDs lead to a wide variety of uses, in research and commercially. QD LEDs (qLEDs) are now on the market as components of electronics with even greater efficiency than traditional semiconductor LEDs. Size-tunability makes qLEDs useful for single-color qLEDs, and blends of QDs can be used to fluoresce with multiwavelength white light. Also on the market are QD TVs. These make use of QDs' narrow-band fluorescence to create fine pixel resolution with brighter, truer colors compared to traditional light filters used in standard LCD sets.

The size-tunable absorption of QDs is currently being studied in solar cells for increasing the usable range of the solar spectrum and the efficiency of photoconversion.[6] One of the primary goals is to find a ligand environment which successfully anchors the QDs to a substrate, allows them to efficiently transfer electrons, and protects them from photooxidation with prolonged use. Potential advantages of QDs over traditional dyes lies in their broad range of tunable absorption while maintaining general physical surface properties. This means that a treatment that works with one size would ideally be applicable to all sizes, and thus all absorption wavelengths; as opposed

to designing individual organic dyes which absorb at each spectral point, and finding a treatment for each one to integrate into the photovoltaic cell. This tunability also makes QDs ideal candidates for light detection in instruments or electronic components. QD photodetectors could potentially be more efficient, sensitive, and specific than the more typical photoresistor or charge-coupled detectors (CCDs) which are currently popular.

QDs are already being used for macro- and microimaging in biology (Figure 7).[7] Their nanometer-scale size, bright fluorescence, and ligating capability makes them useful for fluorescence imaging of both large systems and subcellular systems. As a result of facile surface chemistry, QDs can be functionalized with antigens, aptamers, or other tagging molecules which target specific proteins or regions of a cell. Mixtures of QDs, each tailored to a certain tissue, organelle, protein, *etc.* can be used to stain or dye samples for fluorescence imaging using a single excitation to get a multicolor image.

Because QD fluorescence has been shown to be highly sensitive to ligand environment, they can be used as fluorophores in fluorescence detection experiments, as well. QD fluorescence can be enhanced, quenched, or peak-shifted upon interacting with target molecules, making them useful for chemical detection for research or quality control purposes. This sensitivity can also be used for biological study, as shown by Figure 8, where a QD system showed a significant emission maximum peak shift to shorter wavelengths upon interaction with bacterial spores.[8] QDs have also been used in FRET spectroscopy as both a donor and acceptor fluorophore, favored again because of their phototunability and high fluorescence quantum yields. Chiral nanoparticles have the capability of performing enantiospecific reactions with chiral molecules.[9-15] Studies have seen both fluorescence enhancement and quenching as a result of enantiospecific interactions, displaying the potential for a wide range of detection options.

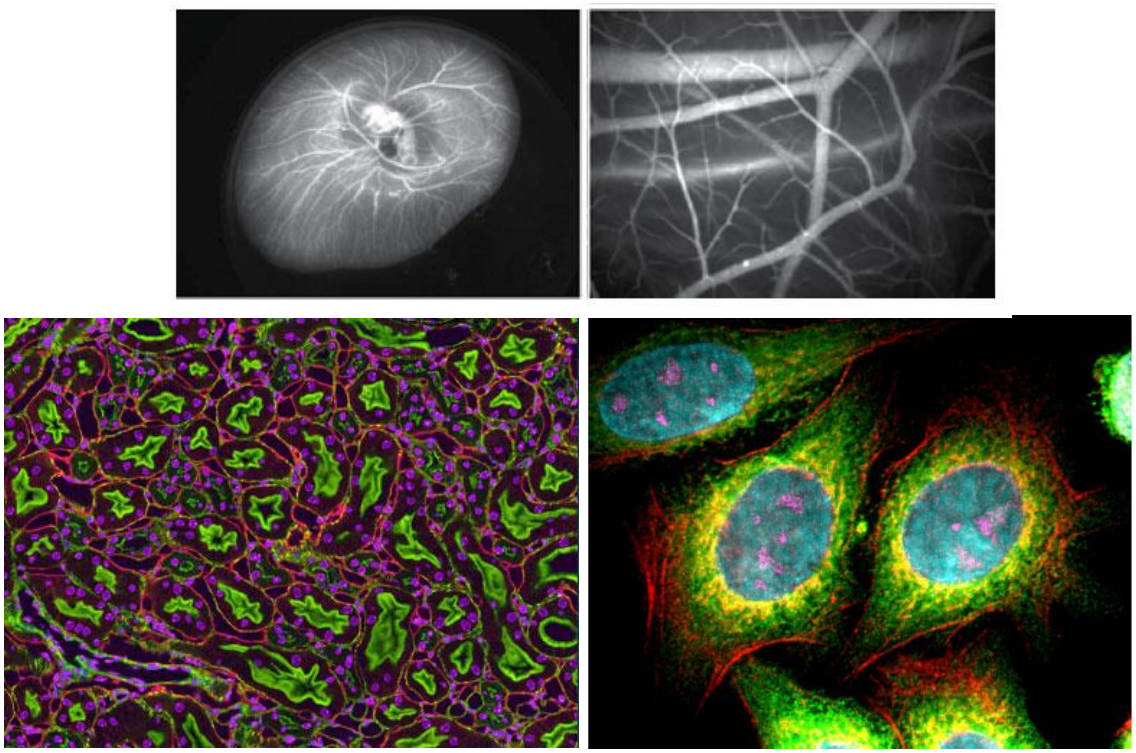

Figure 7: *CdSe-CdTe core-shell QD tagging for fluorescent imaging. QDs have been used to image fine macroscopic systems like chicken embryos (top), tissue samples like mouse liver (bottom left) and subcellular systems (bottom right) in multiple colors through single excitation. Images: Colapinto.*[7]

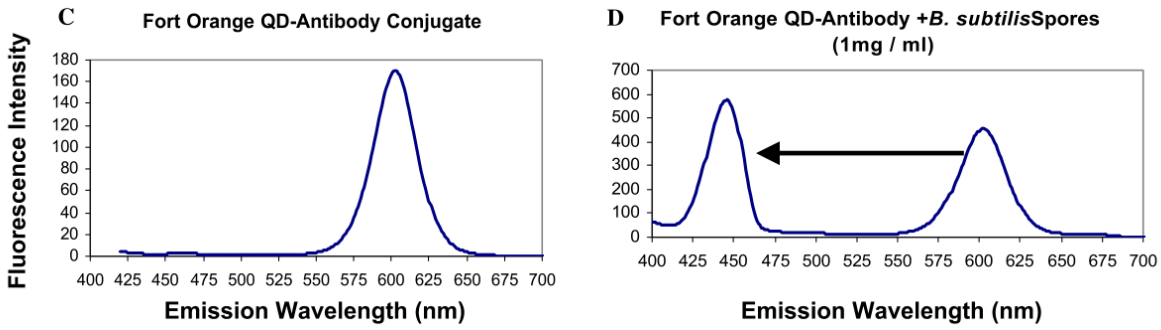

Figure 8: *CdSe-ZnS core-shell QD fluorescence shift upon bacterial binding.*[8] *QDs activated with an antibody conjugate display a single sharp emission peak as is typical. When exposed to bacterial spores with the complimentary antibody, the fluorescence peak experiences a strong blueshift because of the change in ligand environment.*

The first chiral, optically active QDs (CdS) were prepared by the Gun'ko group and coworkers in 2007 using aqueous synthesis in the presence of penicillamine (Figure 9).[16-17] It was believed that a CdS nanocrystal grown in a chiral media resulted in a chiral crystal structure. Further work by the Gun'ko group used *ab initio* modeling to examine the interaction between ligands and the crystal surface. With these studies, it was hypothesized that the core of the QD nanocrystal could be achiral, with only surface modifications imparting chirality. Their models predicted that ligands could coordinate in an enantiospecific manner on the surface of the crystal, and they were capable of distorting the position of surface atoms. They proposed that it was this coordinated distortion that gave rise to the optical activity and appearance of the chiral CD signal.

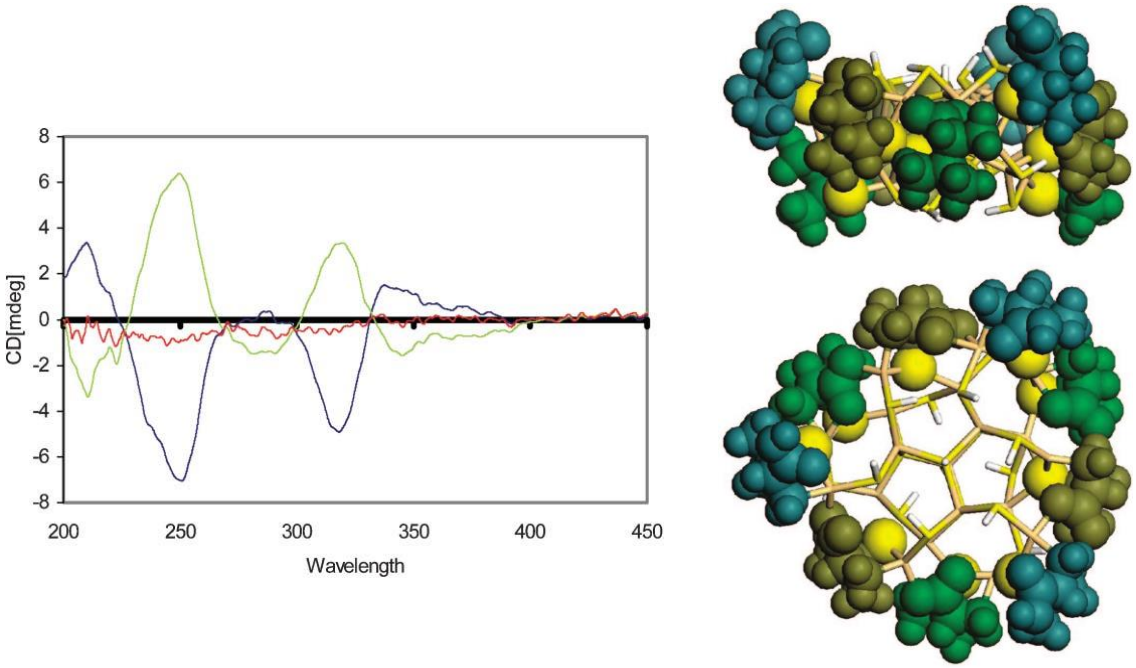

Figure 9: *First study of chiral QDs.[16-17] (Left) CdSe QDs synthesized with aqueous penicillamine exhibited a CD signal at the bandgap absorption region. CdS capped with L- (green) and D-Pen (blue) displayed mirror-image profiles, while CdS capped with racemic mixture of Cys (red) had no CD. (Right) Computational models of enantiomeric penicillamine bound to a sample nanocrystal predicted the coordination of ligand molecules into helical arrangements, while distorting the surface atoms in a chiral manner.*

Kotov and coworkers used a model CdTe crystal to propose a different origin of chirality (Figure 10).[18] Similar to the central chirality exhibited in tetrahedral carbon with four different

substituents, a Cd atom in the CdTe crystal could have four different bonding environments because of ligands and impurities (such as oxygen atoms incorporated into the surface layer of CdTe by oxidation). When these differences were incorporated along with a chiral cysteine (Cys) ligand using an *ab initio* computer model, it was found that the most stable conformation of a system with a chiral ligand depended on the enantiomer of the ligand (L-Cys is more stable in the R-type configuration, while D-Cys prefers the S-type). More recent works support the hypothesis that a chiral crystal structure, through impurities or other defects, plays a part in imparting the chirality of the QD system, along with other factors.[12, 14, 19-21]

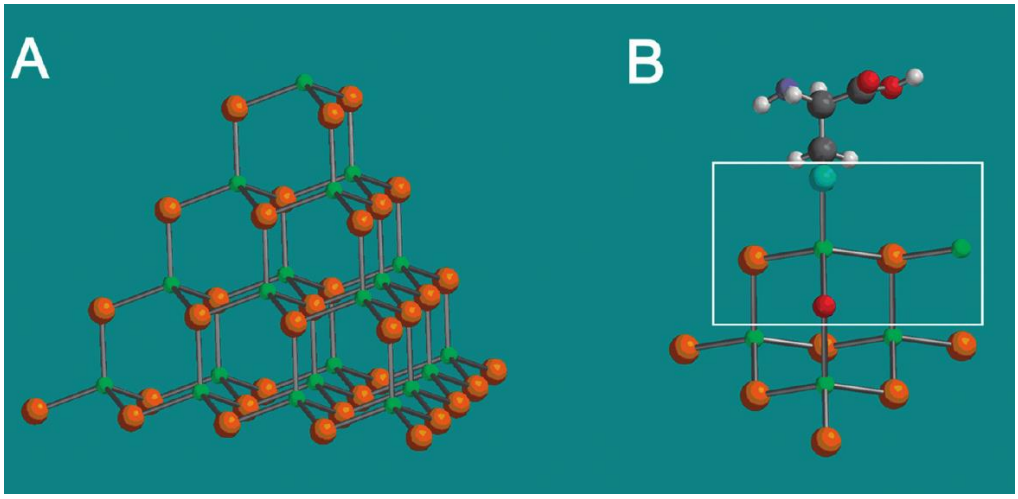

Figure 10: *Collective point chirality.[18] Another proposed theory examined the possibility of point chirality arising from heteroatomic arrangements at the crystal surface, involving ligands and possible defects. A model nanoparticle of CdTe (A) can have point chirality originating from various surface contamination defects (B).*

In 2013, Balaz and coworkers published the first example of QD chirality induced by a post-synthetic ligand exchange on achiral QDs (Figure 11)[5], which will be discussed in more detail later.[5, 22] By starting with achiral CdSe QDs and exchanging the achiral oleic acid capping ligands with chiral cysteine, the resulting optical activity and corresponding CD signal was attributed specifically to the chiral ligand electronic interactions with the QD. It was found that this induced chirality was not permanent, as a second reverse-phase transfer from cysteine to achiral

dodecanethiol (DDT) caused the CD signal to disappear. The work for this thesis began with the continuing study of the phase transfer ligand-induced chirality in achiral QDs. **Our working hypothesis for this project is: the structure of the ligand plays a key role in the induction of chiroptical activity by affecting the binding mode, binding geometry, and binding pattern of the ligand on the crystal surface.** Also, both the nature of the functional groups and their positions within the structure are important.

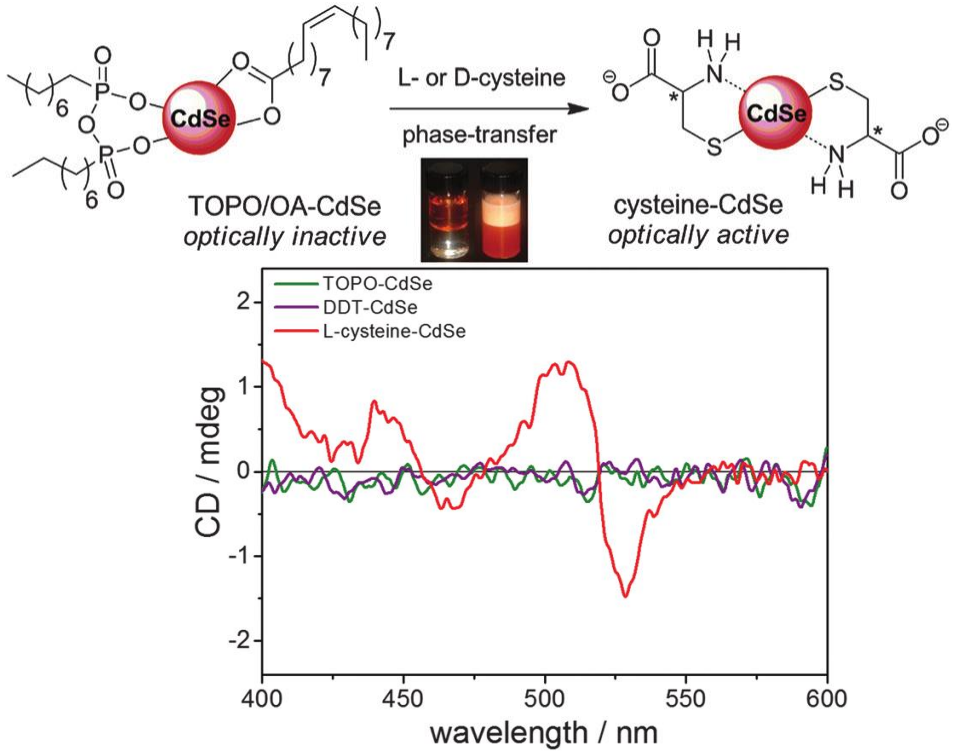

Figure 11: *First example of ligand-induced chirality.[5] (Top) A post-synthetic ligand exchange took achiral TOPO/OA CdSe QDs in organic solution and exchanged the ligands for chiral L-Cysteine in aqueous solution. (Bottom) The CD spectra of the TOPO/OA CdSe showed no chirality (green). After the ligand exchange, aqueous L-Cys CdSe showed bandgap CD spectra (red). A second exchange to achiral DDT showed no chiral memory (purple), indicating that there was no permanent deformation of the crystal structure.*

CHAPTER 2: INDUCED CHIRALITY WITH THIOL-CONTAINING LIGANDS

A phase transfer ligand exchange was introduced by Balaz and Varga in 2013 as a robust and straightforward method for the synthesis of chiral, optically active CdSe QDs.[5] To explore the origin of ligand-induced chirality in achiral QDs, the crystal structure of the QD must be ensured to be achiral. This was achieved by synthesizing CdSe from achiral reagents and in the presence of achiral capping ligands. *i.e.* oleic acid as a ligand and octadecene as a solvent (see Methods and Materials).

The first chiral CdSe QDs prepared by phase transfer ligand exchange procedure[23] were functionalized by L- and D- cysteine. The negatively charged thiolate group of cysteine has affinity for the electron-poor surface cadmium atoms forming a relatively strong sulfur-cadmium bond. The carboxylate functional group of cysteine presents another weaker anchoring point to the surface potentially resulting in possible bidentate surface binding (Figure 12). In order to deprotonate sulfhydryl (SH) and carboxyl (COOH) groups and form more reactive, negatively charged thiolate (S^-) and carboxylate (COO^-), the pH of an aqueous L-Cys solution had to be raised over 8.3, the pK_a of the thiol (Figure 13). The reaction was a phase-transfer ligand exchange, which requires the L-Cys to enter a toluene solution of OA-CdSe before reacting with the QDs. Because a polar molecule has a low diffusion rate in nonpolar solvents, the (+)-charged amine group of L-Cys needed to be deprotonated as well in order to decrease the overall charge of the molecule and increase diffusion and thus the rate of reaction. This meant exceeding a pH of 10.8, the pK_a of the ammonium group.

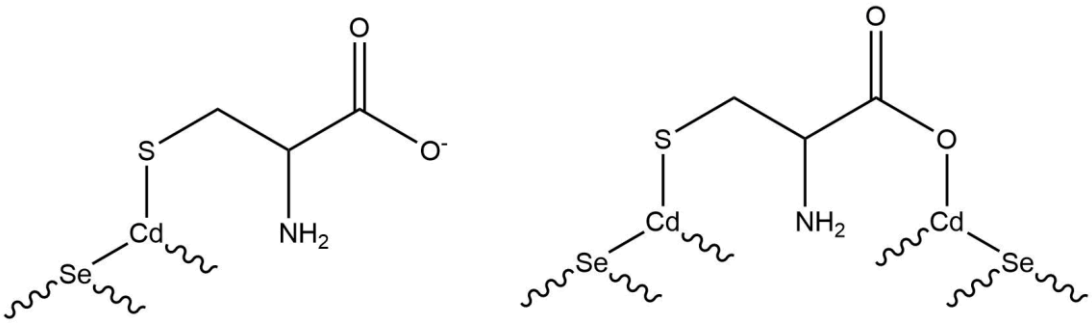

Figure 12: *Cysteine can ligate to the surface of CdSe QDs by monodentate (left) or bidentate (right) interactions.*

Optimizations of QDs functionalized by chiral thiol ligands were performed by prior students. What follows is a brief summary of that work, which was detailed in previous publications.[5] A pH of 12.0 worked best for the ligand exchange with L-Cys and D-Cys. At this pH the cysteine has an overall charge of -1. The negatively-charged and polar thiolate and carboxylate groups however present a potential problem for the phase transfer. To counter this, organic base tetramethylammonium hydroxide (TMAH) was used for pH adjustments. Tetramethylammonium (TMA) is a water-soluble hydrophobic cation that was used to facilitate the transfer of the polar negatively-charged L-Cys into the nonpolar organic phase (*i.e.*, toluene). The TMA cation binds to the charged groups of the L-Cys, neutralizing the charge and providing hydrophobic "caps" which reduce the overall polarity of the molecule and increase its solubility in organic phase.

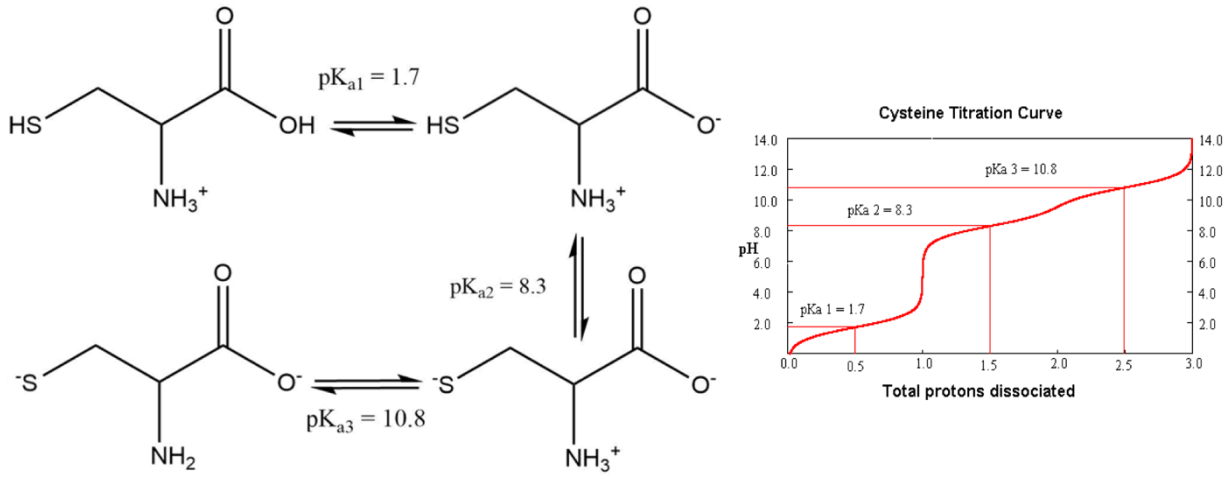

Figure 13: *Cysteine has three acidic protons: the carboxyl (pKa = 1.7), the sulfhydryl (pKa = 8.3), and the ammonium (pKa = 10.7). Graph credit: E.K. O'Neil, New Mexico State University.*

The concentration of the aqueous solution of the ligand was empirically set at 0.056 M (although concentrations as low as 1/10 of this were successfully used for some cysteine derivatives). Instead of optimizing around molar concentration of OA-CdSe, absorbance was held constant at 0.85 to account for size differences between samples. This approach provides an easy-to-use metric for reaction setup. Absorbance and concentration of QDs in the reaction mixture were determined using simple dilution equations, since absorbance directly correlates to concentration according to Beer's Law.

Because colloidal solutions of QDs are light-sensitive and prone to degradative photooxidation, the reaction mixture was deoxygenated using three vacuum-N_2 purge cycles before the reaction continued under N_2 atmosphere in the absence of light. A typical reaction time for successful ligand exchange reaction with cysteines was 18-24 h.

Figure 14: *Phase transfer ligand exchange reaction between OA-CdSe (in toluene) and L-Cys (in water). During the reaction (left) the mixture forms an emulsion. After letting the mixture stand (right), the aqueous phase settles out, containing the newly-formed L-Cys-CdSe as clearly indicated by the color.*

When the decided reaction time was up, stirring was stopped and the phases were allowed to separate for about 1 hour (under N_2, in the dark). Upon separation, the color of the layers visually confirmed that the exchange occurred, with the top organic layer turning white and the bottom aqueous layer gaining the color of the QDs (Figure 14). The bottom layer was removed using a syringe and transferred to centrifuge tubes for purification.

The water-soluble cysteine functionalized CdSe QDs were purified by precipitation and separated by centrifugation. Acetone and ethanol were both used successfully for precipitation. Ethanol was used for the majority of purifications, with the notable exception of *N*-acetyl-L-cysteine. Pure ethanol failed to fully precipitate the *N*-acetyl-L-cysteine functionalized CdSe QDs, so a combination of isopropanol and ethanol was used (pure isopropanol over-precipitated the QDs, making them insoluble in water after centrifugation). A ratio of 8:1 solvent to aqueous solution was found to be most efficient for precipitation, but mixtures with a ratio as low as 5:1 worked. The mixture was centrifuged at approximately 17,500× g for 10 minutes. The supernatant was removed *via* decantation, then the precipitate redissolved in Distilled water (Figure 15).

Figure 15: *L-Cys-CdSe precipitated on the side of the centrifuge tube*

Multiple precipitations were used at times to increase sample purity, which improved CD spectra clarity, but at the cost of sample concentration. Two precipitations were found to be sufficient to give viable samples at sufficient concentration and desirable purity.

Phase transfer reaction volume was varied from 8 mL to 32 mL total volume, with the ratio maintained at 5:3 aqueous to organic volume. Volume was altered based on factors such as scarcity of ligand and amount of sample required. Preliminary reactions exploring new ligands were ran at a small scale to optimize conditions (before being scaled up). QDs were characterized primarily by UV-Vis absorption, emission, and circular dichroism (CD) spectroscopies. UV-Vis gave insight about concentration and size QDs through the empirically-derived Peng equation.[4] Fluorescence spectra were taken, with the excitation wavelength selected based on the absorption spectrum. The second excitonic peak was used for excitation to maximize the measurable range of the fluorescence spectrum, as the emission peak lies close to the first absorption peak (QDs have small Stoke's shift). The aqueous cysteine-capped QDs consistently exhibited a reduction in fluorescent intensity compared to the starting OA-CdSe (*i.e.* ligand exchange induced fluorescence quenching). Fluorescence intensity has been previously shown to be sensitive to ligand environment and concentration.[24] OA-capped QDs exhibited high fluorescence with narrow peak resolution, due to the insulating effect of the long-chain, optically-inactive ligand. Conversely,

cysteine's small size offers less protective separation between the QDs, resulting in increased aggregation. There is also a high likelihood that the ligand exchange process results in random defects on the surface of the QD, creating surface traps. Taken together, these introduce alternative relaxation pathways, either non-fluorescent (*e.g., via* aggregation) or with altered fluorescence (surface traps, indicated by broad fluorescence signal at longer wavelengths), resulting in an overall reduction in band-gap fluorescence intensity.[25]

CD spectroscopy reports a difference in absorption between left-handed and right-handed circularly polarized light. Simply put, a chiral substance preferentially absorbs one direction, thanks to the magnetic induction of an electron that is being excited. When the directional polarity of a transition dipole moment compliments that of the incident light, the light is more easily absorbed, as opposed to an opposing polarity between the two.[15] Chiroptical activity was successfully induced in QDs with a variety of ligands in both CdS and CdSe (Figures 16 – 17).[1] A signal is labeled "positive" or "negative" based on the polarity of the first peak. As expected, opposite enantiomers induced opposite polarities of CD spectra in the QDs (Figure 16a-c). And, notably, *N*-acetyl-L-cysteine give rise to a negative CD signal, while all other L-ligands yielded positive CD signals at excitonic wavelengths (Figures 16e and 17g).

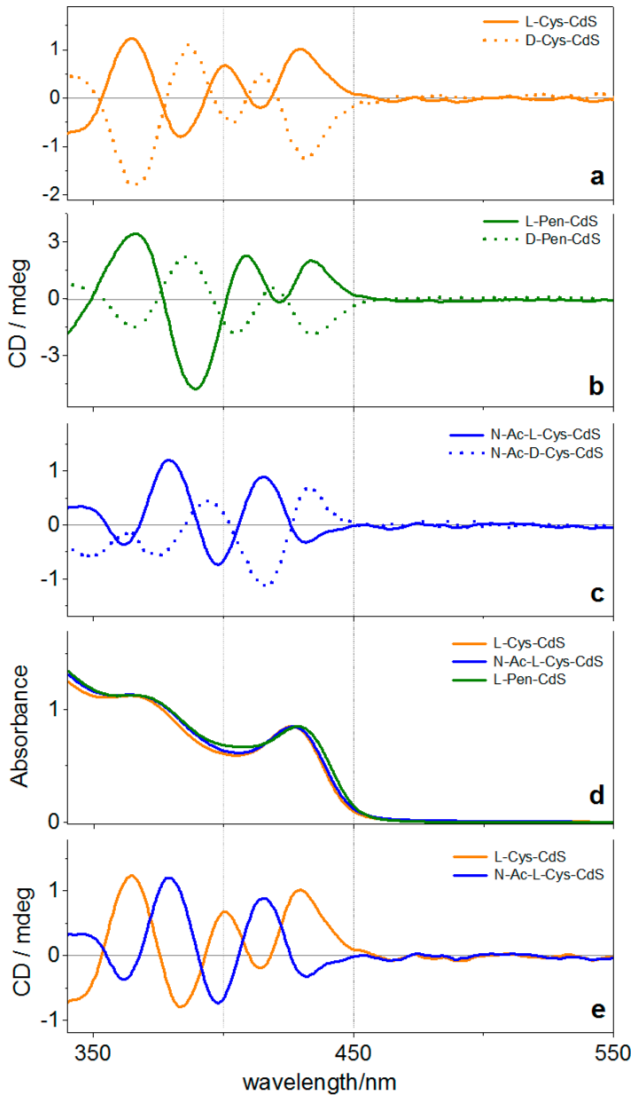

Figure 16: *CD spectra of 4.3 nm CdS functionalized by (a) Cys, (b) Pen, and (c) N-Ac-Cys.*[1] *Enantiomeric pairs result in mirror image CD spectra. All samples produced similar absorption spectra (d) with minimal peak shift. (e) N-Ac-L-Cys produced a mirrored spectrum compared to L-Cys.*

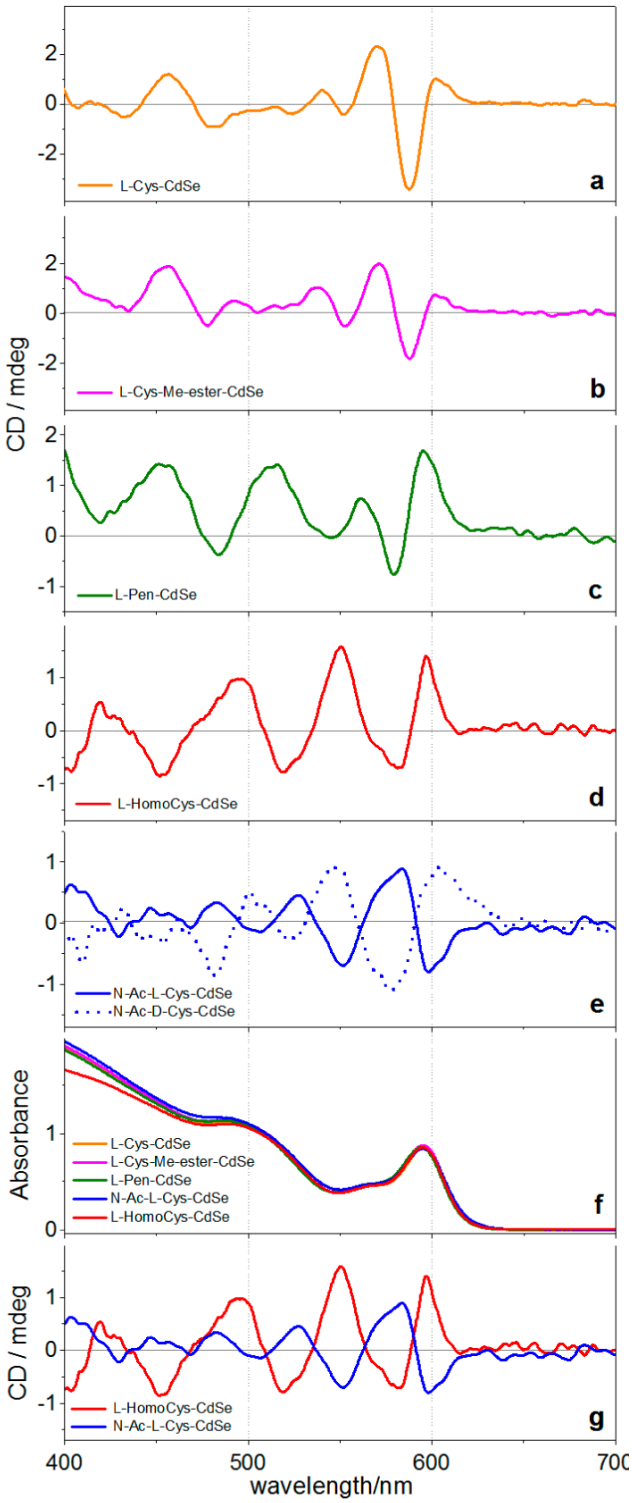

Figure 17: *CD spectra of 4.4 nm CdSe functionalized by (a) L-Cys, (b) L-CysME, (c) L-Pen, (d) L-Homocys, and (e) N-Ac-Cys.[1] All absorption spectra (f) show minimal difference between peaks. (g) N-Ac-L-Cys showed an inverted signal compared to L-Homocys.*

Figure 18 shows that the CD profile does not change polarity with concentration, and the peak intensity increases in a linear relationship with concentration (as does absorption), as expected based on previous work.[26] These experiments helped to exclude aggregation as the main source of chiroptical activity in Cys-capped QDs.

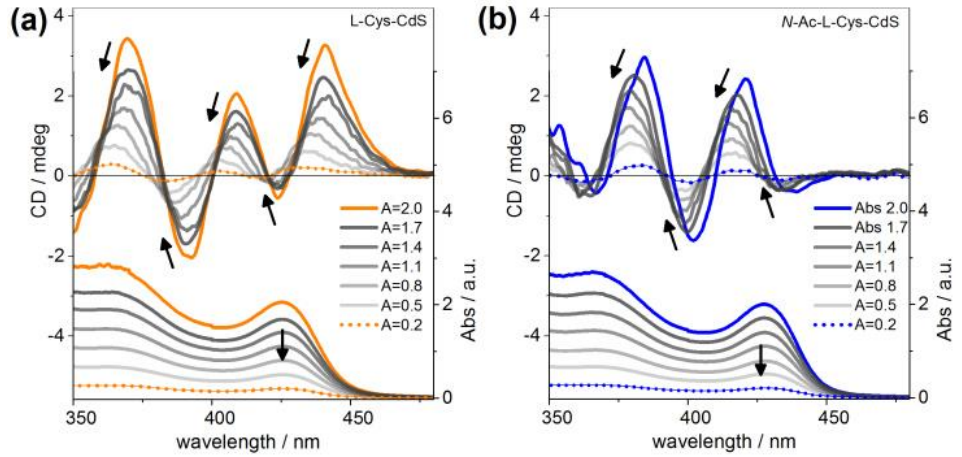

Figure 18: *CD spectra vary with intensity.[1] Absorption peak height and CD peak height decrease in direct proportion with decreasing concentration. This was seen in both (a) L-Cys and (b) N-Ac-L-Cys CdS. [CdS] = from 3.2×10 -6 M to 0.32×10 -6 M*

With the successful induction of chiroptical activity by a chiral capping ligand, the question remained regarding the origin of ligand-induced chirality. It was known that a chiral ligand-induced this response, where an achiral ligand did not. But it didn't necessarily rely on the absolute configuration of the ligand, as shown by the mirror-image spectra of *N*-acetyl-L-cysteine compared to the non-acetylated versions (L-cysteine, L-homocysteine, L-penicillamine). Computational study, performed by Dr. Kubelka (University of Wyoming), aided our understanding by using *ab initio* modeling to predict CD spectra for several systems using the same ligands arranged in different geometric patterns on the crystal surface. The same molecule could produce various signals, even mirrored-polarity peaks, simply by altering its geometric orientation in relation to the surface. Modeling of electronic interactions predicted delocalized HOMO electrons due to orbital hybridization between the CdSe and the ligands.[5] These models also demonstrated a

different mirror image-like binding mode for *N*-Ac-L-Cys, through electrostatic interactions between the acetyl oxygen and surface cadmium (Figure 19).[1] This alternative binding mode could be the cause of the experimentally observed inverted CD signal between L-Cys and *N*-Ac-L-Cys.

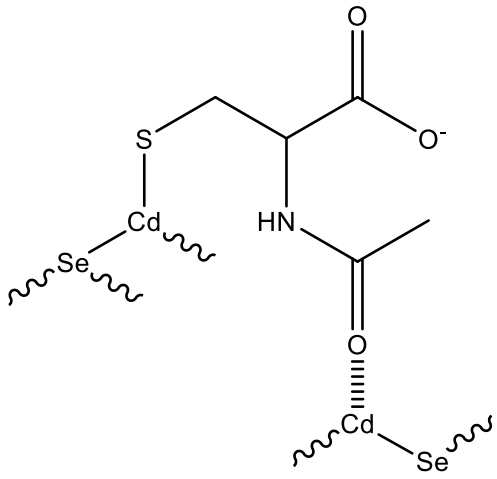

Figure 19: *A potential N-acetyl-L-cysteine binding mode. N-Ac-Cys has three available coordination sites (the thiolate, carboxylate, and the N-acetyl oxygen). While tridentate binding is possible, it is hypothesized that the most stable collective configuration may be bidentate through thiolate and N-acetyl groups. This is supported by calculated and empirical data.*[5]

CHAPTER 3: REACTIONS WITH THIOL-FREE LIGANDS

To further examine ligand induced chirality in QDs, a set of thiol-free ligands was selected as ligand systems. Study began using malic acid (MA), a naturally-occurring dicarboxylic acid containing a chiral center with a hydroxy (-OH) group.

Reaction conditions were selected to mimic those of the thiol-containing ligands with regards to concentrations. Other variables had to be optimized, including the reaction pH (Figure 20). The range of pH values tested ran from 3.0 to 12.0. We hypothesized the optimum pH to be between 3.4 and 5.2, the two pK_a's of malic acid. Within this range, reactions successfully occurred, allowing for further optimization. As the reaction pH extended out of this range, the exchange decreased in efficiency (Figure 21).

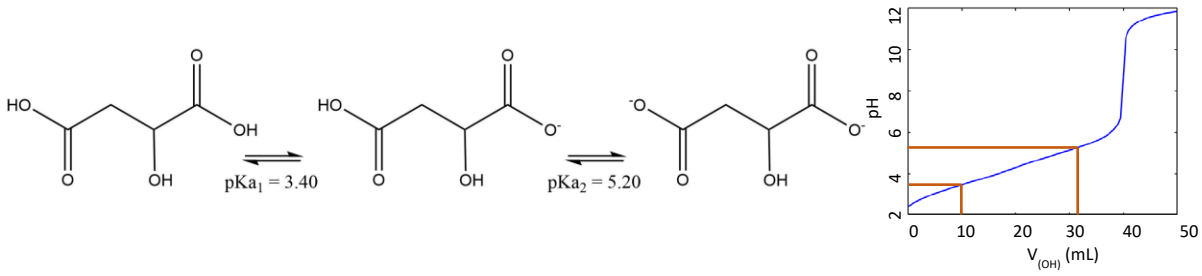

Figure 20: *Malic acid is a dicarboxylic acid with pKa1 =3.40 and pKa2 = 5.20. Titration curve for 0.05 M malic acid with 0.05 M NaOH. Graph credit: Baeza-Baeza.*[27]

Reaction pH below 3.5 and above 5.5 produced minimal exchange as judged by the color of the water layer. Figure 22 is an example of the narrowing-in process of selecting a reaction pH. Starting with a selection of a wide range of solution pH's, they are allowed to react for the same amount of time before comparing their absorption spectra for peak height and location. A high intensity means a greater ligand exchange reaction efficiency, and a peak with minimal shift from the starting OA-CdSe means the QDs are unaffected by the ligand exchange. Through this

narrowing down, we found the optimum pH to be 4.2-4.8 for malic acid, although this varied due to the variability of the starting OA-CdSe. Typically for spectroscopy studies, multiple reactions at several pH values ran in parallel, within ±0.2 of the optimum.

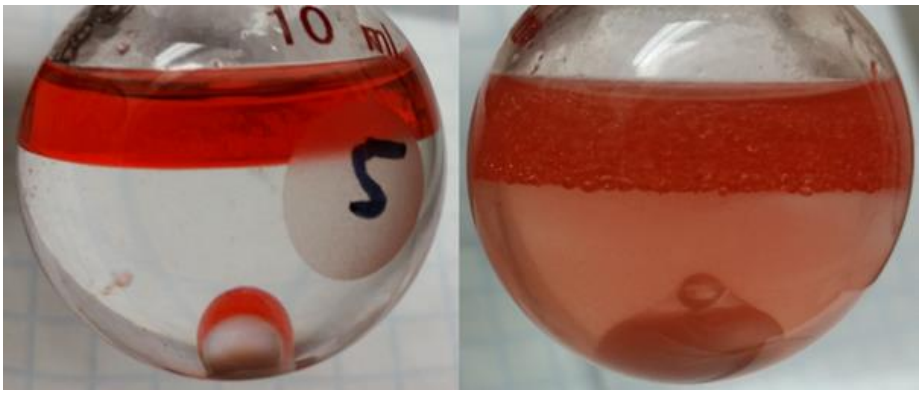

Figure 21: *Reaction pH is a major factor in exchange success, which can be visually determined by the amount of color in the aqueous layer. The aqueous layer of pH 5.5 remained colorless (left), indicating the reaction has failed. A strong aqueous color occurred in a reaction pH of 4.4, (right) indicating successful exchange.*

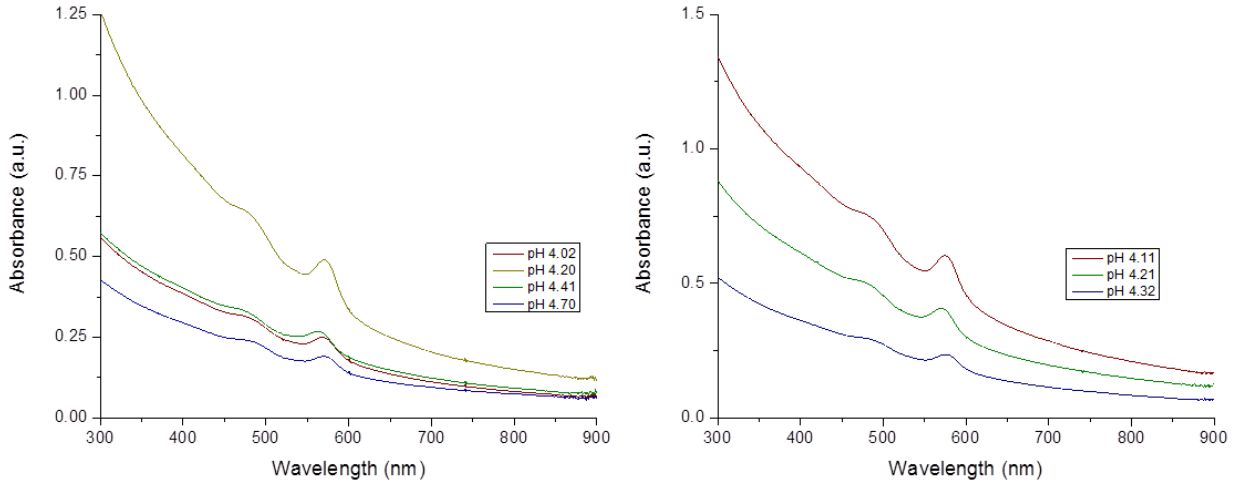

Figure 22: *Optimization of L-MA reaction pH began with a wide range (a) of 4.0-4.7. The best result came from 4.2 (bold dark yellow), as indicated by the strong absorption peak. The pH range was narrowed down around this level (b) and attempted again.*

At this pH, the majority of malic acid was in the mono-deprotonated state, with approximately 90% ionization (either mono- or bis-deprotonated). The reaction pH was adjusted with TMAH, as

with the thiol ligand exchange reactions. As stated earlier, he reaction's pH dependence is due to the balance of reactivity *vs*. solubility of ligand molecules in different phases. A charged species will typically readily diffuse in an aqueous environment. However, the initial ligand exchange occurs in the organic phase, where charged species diffuse much more slowly. A protonated carboxyl will move more easily in the organic solution than would a deprotonated carboxylate group; but it remains less reactive. As mentioned earlier, to aid in the transport, an organic cation such as TMA can balance the charge on the anionic carboxylate, diffuse into the organic solution, and still allow the carboxylate to retain affinity for electron deficient surface Cd atoms. Malic acid can potentially bind to the surface by several binding modes (Figure 23). While initial monodentate binding may take place because of the monodeprotonated form, ultimately bridged bidentate binding would be more energetically favored. The final binding mode is the result of the ligand:QD ratio, ligand structure, and surface structure. Malic acid does have chelating properties, capable of binding both carboxyls to a single cadmium. This could potentially free the cadmium from the surface and lead to degredation of the QD.

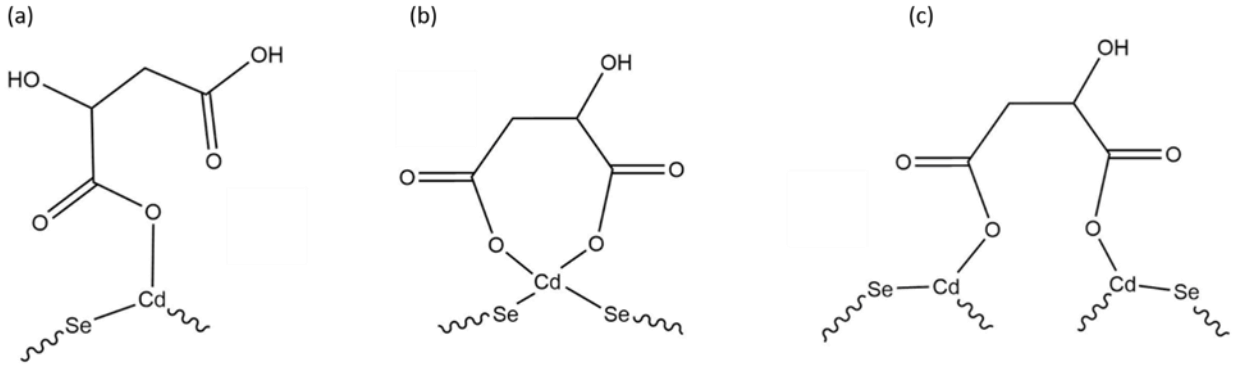

Figure 23: *Binding modes of malic acid to cadmium atoms on QD surface. (a) Monodentate through a single carboxylate; (b) Bidentate on a single cadmium atom; (c) Bidentate bridging two cadmium atoms.*

Reaction time was optimized next by monitoring reactions periodically. Aliquots of aqueous sample were taken and measured with absorptions spectroscopy to quantitatively monitor the reaction progress. However, I observed that these exchanges tend to be sensitive to oxygen, and the repeated opening and sealing/vacuuming negatively impacted the reaction. Flasks were instead visually inspected to compare color transfer and phase development. As seen in Figure 24, the aqueous layer gains color over time, reaching an apparent peak at approximately 2.5-3.0 hours. Under longer reaction times, the acidic conditions promoted QD degradation, causing an apparent absorption peak broadening and blue shift. This degradation can be seen in Figure 24 as the lightening of color from beginning to end. To maximize the yield of carboxylic acid functionalized CdSe QDs, a standard reaction time of 2 hours was used.

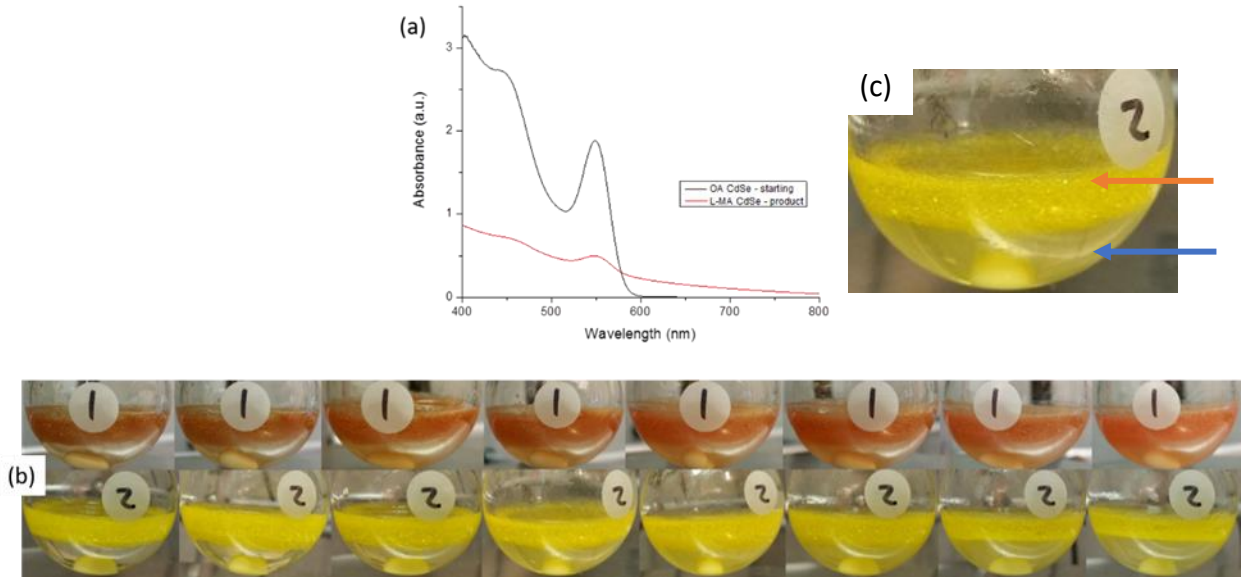

Figure 24: *(a) When reaction times were kept to 2 hours or less, there was relatively little shift (< 2 nm) between the peaks of OA-CdSe (black) and L-MA CdSe (red). (b) L-MA reactions with 4.6 nm (top row) and 2.3 nm (bottom row) CdSe. Reactions were photographed every 30 min for a total of 240 min. (c) The top layer of the reaction is the toluene containing OA-CdSe, while the bottom layer is the aqueous solution of L-MA. The aqueous layer begins colorless, becoming opaquely colored as the ligand exchange proceeds and QDs transition phases.*

The carboxylic acid ligand exchange reactions behaved differently than the thiol reactions. Instead of forming an emulsion, upon injection the organic layer remained distinctly atop the aqueous layer. By the end of the reaction, an 'intermediate phase' formed between the organic and aqueous layer. But if the entire contents of the flask were transferred to a tube, the layers became more distinct (Figure 25b). The toluene layer lost most or all of its color, indicating the QDs had transitioned out of the pure organic phase. The aqueous layer had color in itself, however a large fraction of the QDs were retained in string-like structures within the water.

(a)  (b)

Figure 25: *(a) L-TA- (left) and L-MA-CdSe (right) CdSe aggregating in the cuvette after measurement. (b) Post-reaction mixtures separate into layers.*

To explore the makeup of these layers, they were separated and precipitated individually using the same process as with the thiols: by mixing with a 5:1 ratio of ethanol to aqueous solution then centrifuging at 17,500× *g* for 10 minutes. The organic layer resulted in little precipitate, which when redissolved in toluene and measured confirmed the nearly complete transfer of OA-CdSe from this phase. The aqueous layer gave a precipitate which, as expected, redissolved well in Distilled water. The QDs precipitated from the intermediate layer did not redissolve in either Distilled water or toluene. Yield calculations revealed that the organic phase retained 2-12% of the

QDs, while the aqueous phase gained 10-20%. This means that ~70% of the QDs were either trapped in the intermediate phase, decomposed, or were lost in the purification process.

Long-term solution stability was a notable issue that arose with the carboxylic acids. Whereas Cys-CdSe QDs were stable for days, the solutions of MA-CdSe often began to aggregate within few hours of purification. Attempts were made to minimize the effects of degradation or aggregation including pH adjustment, sonication, temperature changes (heating or cooling), and addition of secondary ligands (such as cysteamine). Unfortunately, none of the experiments resulted in better solution stability of carboxylic acid capped CdSe QDs. Measurement, then, took place immediately after purification, with the sample carefully monitored to ensure its viability for the duration of the spectroscopic process (Figure 25a).

The CD spectra shift according to the absorption spectra and size of the QD, as seen in Figure 26. Because CD is based on the absorption of the sample, as the QD diameter increases, the absorption peak experiences a red-shift, as does the CD peak location. The polarity of the signal remains the same regardless of size, (+/-/+/-; from longer to shorter wavelengths) for L-MA-CdSe and the mirror image (-/+/-/+) for D-MA-CdSe.

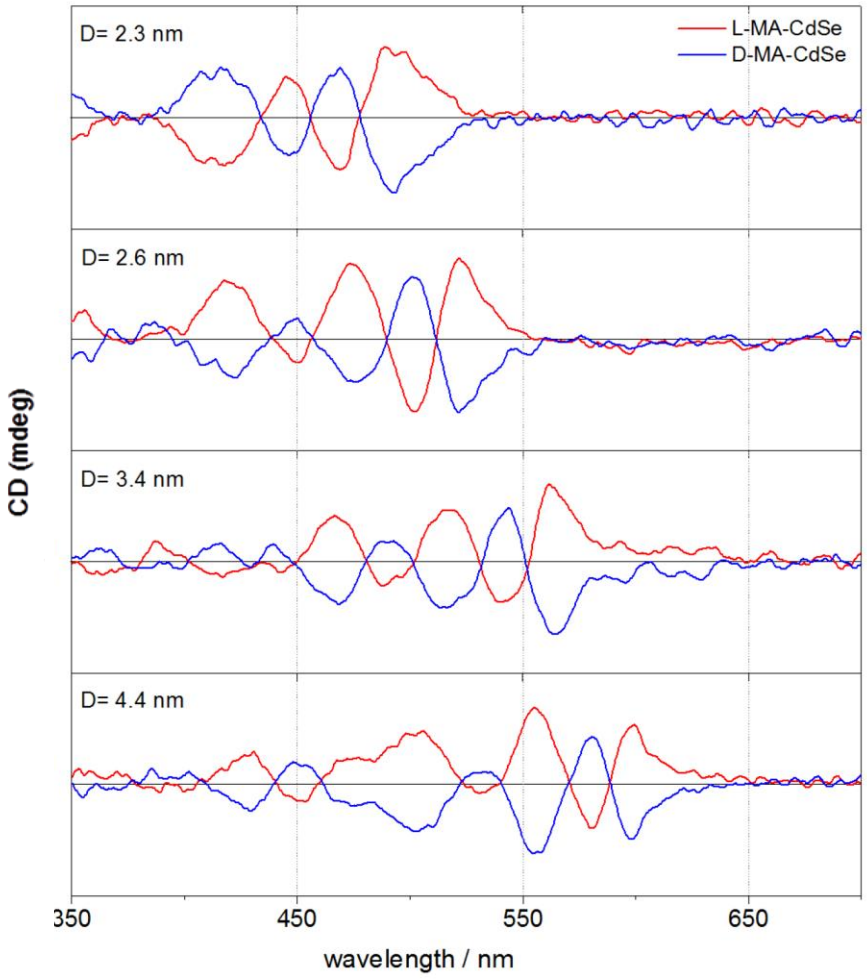

Figure 26: *CD spectra of L- and D-malic acid CdSe functionalized CdSe QDs with different diameters (2.3 nm, 2.6 nm, 3.4 nm and 4.4 nm). The absorption spectra show the size-related peak location, a shift that is also seen in the CD spectra.*

There are several stark contrasts between the thiol-containing cysteine and thiol-free malic acid ligand exchange reactions. The pH used (12.0 and 4.3, respectively) create different ionization states between the two. Cysteine was trisdeprotonated, with (-)-charged carboxylate and thiolate groups and no charge on the amine for an overall -2 charge. Malic acid had a single deprotonated carboxylate, with a total -1 charge (no opportunities for a positive charge). Both have a single carboxylate immediately available for binding, although based on bond strength, cysteine's thiolate will bind first.

With malic acid successfully inducing chirality in CdSe, we decided to explore structurally similar ligands tartaric acid (TA) and aspartic acid (Asp). Tartaric acid produced a reaction with strong absorption and CD signal (Figure 27). Tartaric acid is similar in structure to malic acid, with the addition of another -OH group on C_β. It reacted over a pH range of 3.5-4.1. The CD profile of L-TA-CdSe is opposite that of L-MA. This can be explained as a result of nomenclature, as L-MA and L-TA have opposite absolute configurations (*S*-MA vs *R,R*-TA).

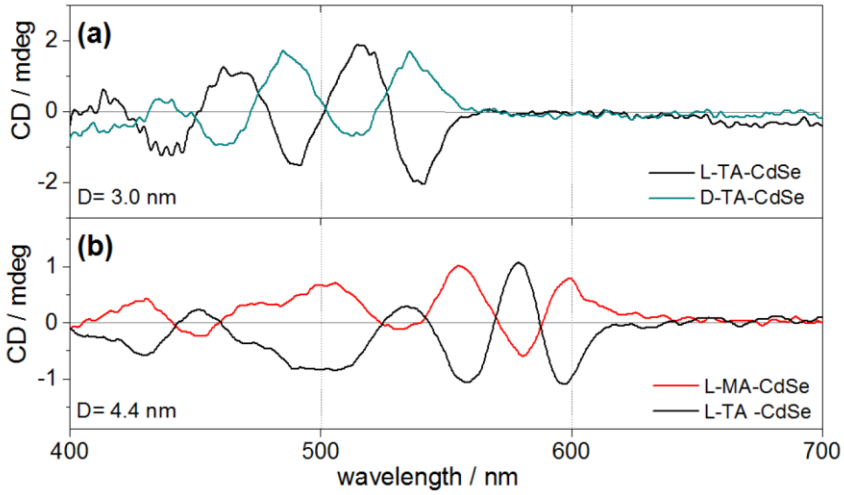

Figure 27: *(a) CD spectra of L- and D-tartaric acid CdSe show the presence of chiroptical signal, with mirror-image spectra between the enantiomers. (b) L-TA has a mirror-image profile compared to L-MA.*

Ligand exchange with aspartic acid was attempted at a pH range of 3.8-4.8, L-aspartic acid resulted in a lower yield of the phase-transfer ligand exchange than malic acid. The L-Asp-CdSe QDs did not exhibit any CD signal. A summary of the ligands discussed is found in Table 1.

Table 1: *Summary of thiol-free ligands used.*

Capping ligand	Enantiomers	pKa	Optimum pH range	CD
MA	L/D	3.40, 5.20	4.2 – 4.8	Yes
TA	L/D	2.98, 4.34	3.5 – 4.1	Yes
Asp	L	1.99, 3.90, 9.90	3.8 – 4.2	No
N-Ac-Asp	L	3.37, 4.91	4.4 – 4.8	Yes

Comparing the ligands which successfully induced chiroptical activity (MA and TA) with ligands that did not (Asp), commonalities can be seen – specifically the possibility for tridentate binding for MA and TA. Aspartic acid has only two carboxylate binding sites available. Without strong tridentate binding, it would be difficult for molecules to arrange in a coordinated manner on the surface of the QD. The addition of the *N*-acetyl group could solve that problem, as it was seen from the thiolate experiments that an acetyl group (CH_3CO) carbonyl coordinates to surface Cd. To test our hypothesis, we introduced an *N*-acetyl group on the amino group of Asp prior to the ligand exchange. *N*-acetyl-L-aspartic acid reacted and produced CD signal (Figure 28). With this group present in *N*-acetyl-L-aspartic acid, the molecule can successfully have tridentate binding. Increased bond order means an increased binding strength and the ability to coordinate ligation across the QD surface, successfully inducing a CD signal. The molecular structures of the thiol-free ligand systems examined can be found in Figure 29.

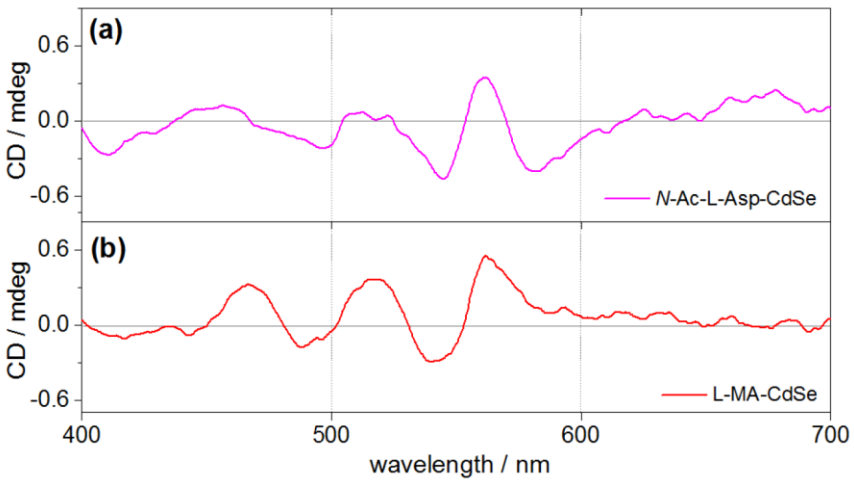

Figure 28: *CD spectra of 3.4 nm CdSe capped with (a) N-Ac-L-Asp and (b) L-MA. Both share many features which line up in the spectra, with the exception of the initial negative peak present with N-Ac-L-Asp.*

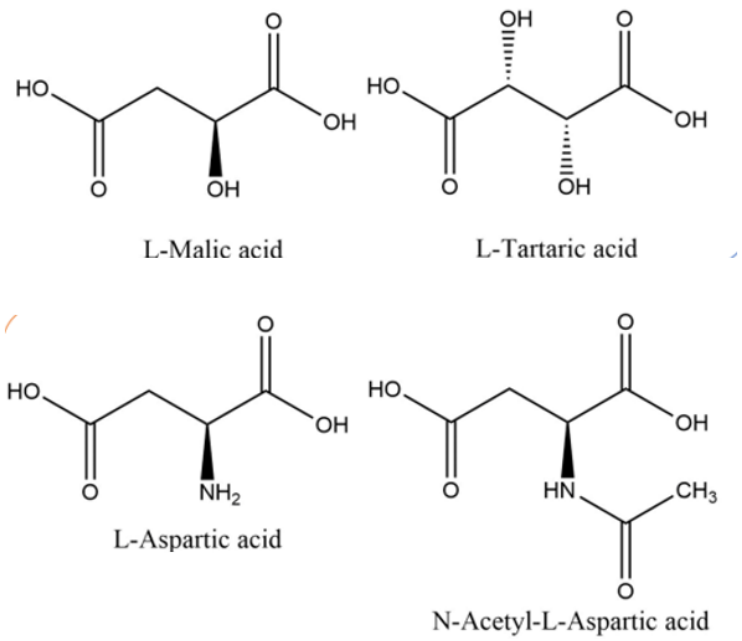

Figure 29: *Molecular structures of the chiral ligand systems examined.*

CONCLUSION

Chiroptical activity can be induced in achiral QDs *via* a post-synthetic ligand exchange with chiral ligands. The polarity of the resulting CD signal is sensitive to the binding geometry of the ligand to the surface of the QD. Thiolate and carboxylate binding can occur with surface Cd atoms, and it is suspected that acetyl oxygen allows for an alternative coordination. It is hypothesized that the chiroptical activity is due to the hybridization of electronic orbitals between the chiral ligand and the achiral QD, and not necessarily from any physical atomic distortion. Varying functional groups of ligands impacts the presence and shape of a CD signal, indicating another factor in addition to geometry for the induction of chiroptical activity.

Further research in varying ligand binding groups, backbone structure, and functional groups could further elucidate the origin and nature of ligand-induced chirality. Practical experimentation along with computational modeling can help us to learn what is required of a ligand system to induce chirality, such that rational design of chiral nanoparticles is possible. Applications for these designed systems could include chemical detection and fluorescence imaging, or novel uses not yet proposed. Increasing our understanding of chiral ligand systems, too, lends knowledge to the study of ligand systems as a whole, with the potential to impact research in energy, medicine, electronics, or other fields where QDs could play a future role.

CHAPTER 4: METHODS AND MATERIALS

CdSe Synthesis, Purification, and Characterization

Procedure for hot-injection CdSe synthesis is modified from previous publication.[1]

Cadmium oxide (CdO), oleic acid (OA), octadecene (ODE), selenium (Se), trioctylphosphine (TOP), and toluene were purchased from Sigma-Aldrich. 200-proof ethanol was purchased from Fisher Scientific.

A mixture of CdO (0.08 g) with OA (10.0 mL) and ODE (17.0 mL) was deoxygenated in a 3-neck flask, then stirred under a nitrogen atmosphere (1700 RPM, 25.5 x 8 mm stir bar). The mixture was heated to 300 °C using a heating mantle wrapped in an insulating blanket. The TOPSe mixture was prepared with Se (0.10 g), TOP (2.1 mL) and ODE (10.0 mL), deoxygenated, then sonicated under nitrogen atmosphere for 5 min. The TOPSe mixture was injected into the hot CdO mixture, then poured into waiting toluene (40 mL) chilled to -20 °C at the desired time to cool and halt the reaction. Reaction time was varied from 4 to 135 sec to get a size range from approx. 2.25 to 4.75 nm in diameter. The absorption spectrum of the crude product was taken to estimate the QD size, but accurate measurement was done after purification.

10 mL of raw QD solution were measured into each of 4 centrifuge tubes (50 mL), followed by 30 mL of 200-proof ethanol for each. The tubes were centrifuged (Beckman J2 centrifuge, JA-20 rotor) at 12,000 RPM (17,400g) for 10 minutes to precipitate the QDs. After all the raw solution was precipitated, it was redissolved in 10 mL of toluene. This was then precipitated again and redissolved in 10 mL toluene.

To characterize the QDs, absorption and fluorescence spectra were collected for serial 5 µL titrations of the purified QD solution into 2 mL of neat toluene. Using the data obtained, the diameter and concentration of the QD solutions could be calculated with the Peng equation.[4]

Phase-transfer Ligand Exchange

Reaction conditions for ligand exchanges are optimized specifically for the ligand being used. Generally speaking, an aqueous solution of the ligand is made in a 25 mL round bottom flask. Typically the concentration is 61 mM in a 5 mL solution. The pH is adjusted to the reaction level using tetramethylammonium hydroxide. In the case where a more acidic pH is required, HCl is used. With some ligands which have limited solubility in water (below 61.3 mM) TMAH is added until the ligand fully dissolves, then the pH is adjusted with HCl. After the aqueous solution is prepared, it is deoxygenated while stirring with a 12.4 mm stir bar at 1700 RPM, and held under a nitrogen atmosphere for the duration of the reaction. The deoxygenation process consists of exposing to a vacuum (<0.2 mbar) for 15 seconds, followed by a nitrogen atmosphere for 60 seconds. This cycle is repeated for a total of 3 times.

The OA QD solution is prepared separately with a syringe. The amounts required are calculated using the concentration data from the microtitrations. 3 mL of a solution with absorbance of 2.0 A.U. is prepared and injected into the deoxygenated aqueous solution. The deoxygenation process is repeated in its entirety, then the flask is covered with aluminum foil and left under nitrogen atmosphere while the reaction occurs. Reaction times varied between 1.5 to 12 hours, depending on the ligand used.

After the reaction is finished (determined by monitoring the color exchange between the phases, and confirmed with aliquot samples from each), the phases are allowed to separate for 5-

30 min. The aqueous layer is removed using a 3 mL syringe without disturbing the layer separation, and placed in a centrifuge tube along with 200-proof ethanol in an 8:1 ratio of ethanol:QD solution. This is centrifuged at 17,400xg for at least 10 minutes. Some ligand systems require more centrifugation time. Others (notably *N*-Ac-Cys) will not precipitate in pure ethanol. In these cases, a mixture of ethanol with isopropanol in a ratio of 2:1, respectively.

After centrifugation, the supernatant is removed with a pipette. The precipitate is then redissolved in distilled water. Typically a minimal amount of water is used to get the strongest concentration possible. For the cuvette used in these experiments, the minimum volume for measurement is 1.6 mL. The newly dissolved QDs are removed with a pipette and characterized with UV-Vis, fluorescence, and CD spectroscopy.

LIST OF REFERENCES

1. Choi, JK., Haynie, B.E., Tohgha, U., Pap, L., Elliott, K.W., Leonard, B.M., Dzyuba, S.V., Varga, K., Kubelka, J., Balaz, M., Chirality Inversion of CdSe and CdS Quantum Dots without Changing the Stereochemistry of the Capping Ligand. *ACS Nano* **2016,** *10*, 3809–3815.

2. Kambhampati, P., Unraveling the Structure and Dynamics of Excitons in Semiconductor Quantum Dots. *Acc. Chem. Res.* **2010,** *44*, 1-13.

3. Murray, C.B., Norris, D.J., Bawendi, M.G., Synthesis and characterization of nearly monodisperse CdE (E = sulfur, selenium, tellurium) semiconductor nanocrystallites. *J. Am. Chem. Soc.* **1993,** *115*, 8706-8715.

4. Yu, W.W., Qu, L., Guo, W., Peng, X., Experimental Determination of the Extinction Coefficient of CdTe, CdSe, and CdS Nanocrystals. *Chem. Mater.* **2003,** *15*, 2854-2860.

5. Tohgha, U., Deol, K.K., Porter, A.G., Bartko, S.G., Choi, J.K., Leonard, B.M., Varga, K. Kubelka, J., Muller, G., Balaz, M., Ligand Induced Circular Dichroism and Circularly Polarized Luminescence in CdSe Quantum Dots. *ACS Nano* **2013,** *12*, 11094-11102.

6. Selinsky, R.S., Ding, Q., Faber, M.S., Wright, J.C., Jin, S., Quantum dot nanoscale heterostructures for solar energy conversion. *Chem. Soc. Rev.* **2013,** *42*, 2963-2985.

7. Colapinto, P., Qdot Imaging, accessed 2017

8. Dwarakanath, S., Bruno, J.G., Shastry, A., Phillips, T., John, A., Kumar, A., Stephenson, L.D., Quantum dot-antibody and aptamer conjugates shift fluorescence upon binding bacteria. *Biochem. Biophys. Res. Comm.* **2004,** *325*, 739-743.

9. Wang, Y., Xu, J., Wang, Y., Chen, H., Emerging chirality in nanoscience. *Chem. Soc. Rev.* **2013,** *42*, 2930-2962.

10. Hu, T., Isacoff, B.P., Bahng, J.H., Hao, C., Zhou, Y., Zhu, J., Li, X., Wang, Z., Liu, S., Xu, C., Biteen, J.S., Kotov, N.A., Self-Organization of Plasmonic and Excitonic Nanoparticles into Resonant Chiral Supraparticle Assemblies. *NanoLett.* **2014,** *14*, 6799-6810.

11. Govan, J.E., Jan, E., Querejeta, A., Kotov, N.A., Gun'ko, Y.K., Chiral luminescent CdS nano-tetrapods. *Chem. Comm.* **2010,** *46*, 6072-6074.

12. Govorov, A.O., Gun'ko, Y.K., Slocik, J.M., Gerard, V.A., Fan, Z., Naik, R.R., Chiral nanoparticle assemblies: circular dichroism, plasmonic interactions, and excitonic effects. *J. Mater. Chem.* **2011,** *21*, 16806-16818.

13. Guerrero-Martinez, A., Alonso-Gomez, J.L., Auguie, B., Cid, M.M., Liz-Marzan, L.M., From individual to collective chirality in metal nanoparticles. *Nano Today* **2011,** *6*, 381-400.

14. Ben-Moshe, A., Maoz, B.M., Govorov, A.O., Markovich, G., Chirality and chiroptical effects in inorganic nanocrystal systems with plasmon and exciton resonances. *Chem. Soc. Rev.* **2013,** *42*, 7028-7041.

15. Ben-Moshe, A., Markovich, G., Chiral Ligand-Induced Circular Dichroism in Excitonic Adsorption of Colloidal Quantum Dots. *Isr. J. Chem.* **2013,** *52*, 1104-1110.

16. Moloney, M.P., Gun'ko, Y.K., Kelly, J.M., Chiral highly luminescent CdS quantum dots. *Chem. Comm.* **2007,** *38*, 3900-3902.

17. Elliott, S.D., Moloney, M.P., Gun'ko, Y.K., Chiral Shells and Achiral Cores in CdS Quantum Dots. *NanoLett.* **2008,** *8*, 2452-2457.

18. Zhou, Y., Yang, M., Sun, K., Tang, Z., Kotov, N.A., Similar Topological Origin of Chiral Centers in Organic and Nanoscale Inorganic Structures: Effect of Stabilizer Chirality on Optical Isomerism and Growth of CdTe Nanoparticles. *J. Am. Chem. Soc.* **2010,** *132*, 6006-6013.

19. Govorov, A.O., Fan, Z., Hernandez, P., Slocik, J.M., Naik, R.R., Theory of Circular Dichroism of Nanomaterials Comprising Chiral Molecules and Nanocrystals: Plasmon Enhancement, Dipole Interactions, and Dielectric Effects. *NanoLett.* **2010,** *10*, 1374-1382.

20. Mukhina, M.V., Maslov, V.G., Baranov, A.V., Fedorov, A.V., Orlova, A.O., Purcell-Milton, F., Govan, J., Gun'ko, Y.K., Intrinsic Chirality of CdSe/ZnS Quantum Dots and Quantum Rods. *NanoLett.* **2015,** *15*, 2844-2851.

21. Moloney, M.P., Govan, J., Loudon, A., Mukhina, M., Gun'ko, Y.K., Preparation of chiral quantum dots. *Nat. Protoc.* **2015,** *10*, 558-573.

22. Tohgha, U., Varga, K., Balaz, M., Achiral CdSe quantum dots exhibit optical activity in the visible region upon post-synthetic lgiand exchange with D- or L-cysteine. *Chem. Comm.* **2013,** *49*, 1844-1846.

23. Anderson, N.C., Hendricks, M.P., Choi, J.J., Owen, J.S., Ligand Exchange and the Stoichiometry of Metal Chalcogenide Nanocrystals: Spectroscopic Observation of Facile Metal-Carboxylate Displacement and Binding. *J. Am. Chem. Soc.* **2013,** *135*, 18536-18548.

24. Teunis, M.B., Dolai, S., Sardar, R., Effects of Surface-Passivating Ligands and Ultrasmall CdSe Nanocrystal Size on the Delocalization of Exciton Confinement. *Langmuir* **2014,** *30*, 7851-7858.

25. Noh, M., Kim, T., Lee, H., Kim, C.K., Joo, S.W., Lee, K., Fluorescence quenching caused by aggregation of water-soluble CdSe quantum dots. *Colloid Surface A* **2010,** *359*, 39-44.

26. Ben-Moshe, A., Szwarcman, D., Markovich, G., Size Dependence of Chiroptical Activity in Colloidal Quantum Dots. *ACS Nano* **2011,** *5*, 9034-9043.

27. Baeza-Baeza, J.J., Perez-Pla, F.F., Garcia-Alvarez-Coque, M.C., Teaching Chemical Equilibria Using Open Source Software OCTAVE. *World J. Chem. Ed.* **2015,** *3*, 127-133.